A Modular Bio-Platform Based on a Versatile Supramolecular Multi-Enzyme Complex Directly Attached to Graphene

Abeer Alshammari[1,2,3‡], Mareike G. Posner[1,4‡], Abhishek Upadhyay[1,4], Frank Marken[5], Stefan Bagby[1,4]*, and Adelina Ilie[1,2]*

[1] Centre for Graphene Science, University of Bath, Bath, BA2 7AY, UK

[2] Department of Physics, University of Bath, Bath, BA2 7AY, UK

[3] Department of Physics, King Saud University, Riyadh 11451, Saudi Arabia

[4] Department of Biology and Biochemistry, University of Bath, Bath, BA2 7AY, UK

[5] Department of Chemistry, University of Bath, Bath, BA2 7AY, UK

Corresponding Author

*Adelina Ilie, email: a.ilie@bath.ac.uk, *Stefan Bagby, email: bsssb@bath.ac.uk

1. Protein purification. After protein purification the correct size of recombinant proteins and purity was assessed by SDS-PAGE. E1 is a hetero-tetramer composed of two alpha and two beta chains ($\alpha_2\beta_2$). The predicted molecular weights for the alpha and beta chains are 41 and 37 kDa, respectively.[1] The predicted molecular weight for the E2 monomer is 47 kDa.[1] These values compare favourably with the molecular weight determined by SDS-PAGE as shown in Figure S1.
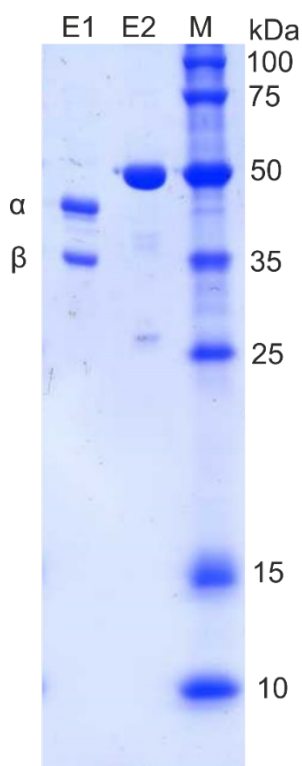

Figure S1: SDS-PAGE (15% gel) of purified E1 and E2. Lane M shows the molecular weight markers for reference.

2. Distribution of polar/non-polar sequences in the *T. acidophilum* E2 monomer. Amino acid residues 1 to 400 are shown in single letter code (Figure S2). Relative solvent accessibility is shown in shades of grey starting from black (0, completely buried inside protein structure) to white (9, fully exposed to environment). Secondary structure elements (red zigzag - helix; green arrow - sheet, blue line - coiled) are indicated. Physical-chemical properties: hydrophobic (light yellow: A,C,F,G,I,L,M,P,V), polar (salmon: N,Q,S,T), charged (light and dark red: D,E-neg; R,K-pos), amphipathic (dark yellow: H,W,Y). (Data generated using Polyview 2D).[2]
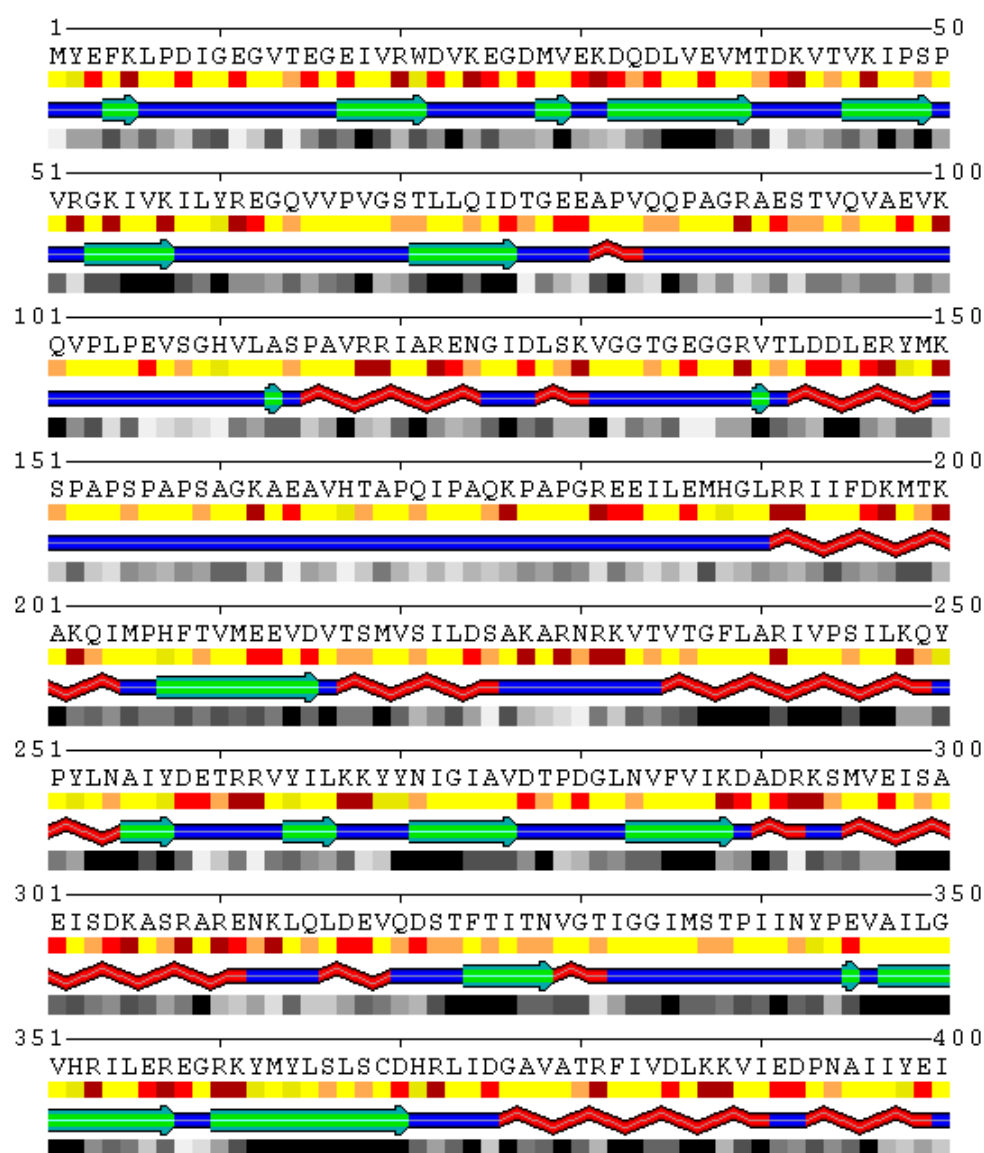
Figure S2: Overview of E2 monomer sequence (excluding the His-tag), structure, chemical properties of amino acids, and relative solvent accessibility.

3. Cryo-EM images of the assembled 60-mer E2 complex of *T. acidophilum* 2-OADHC. The collage in Figure S3 shows different views: individual complexes (A, B), the classums (C, D) and the rotationally averaged classums (E, F). In the last column, from top to bottom: image 6 is a view along the fivefold symmetry axis of the dodecahedron from Figure 1, main text, revealing one of its pentagonal faces; image 12 reveals the 10-vertex projection of the dodecahedron also obtained by viewing it along the fivefold symmetry axis but at a different focus than for image 6; image 18 is a "cart wheel view" of a vertex between three adjacent pentagonal faces, i.e. along the threefold symmetry axis; while image 24 is a tilted fivefold/threefold view.
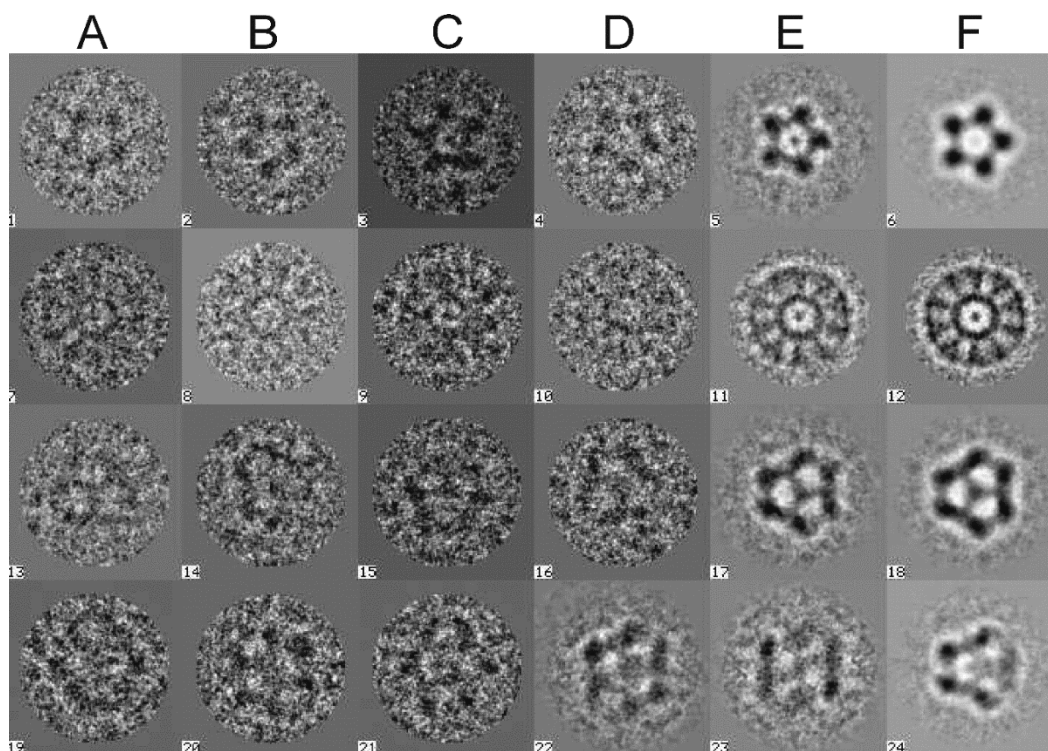
Figure S3: *Cryo-EM images of the assembled 60-mer E2 complex of T. acidophilum 2-OADHC: (A-B) individual particles, (C-D) the classums, and (E-F) the rotationally averaged classums.*

4. Quantitative characterization of an E2 complex biomolecular monolayer formed on graphenic surfaces. One assumes uniform monolayer coverage with 60mer E2 complexes, where one E2 complex is 2.79 megadaltons. If each complex is 17 nm across when supported by a graphene surface (as discussed in the main text), then we have approximately 10^7 nm / 17 nm E2 complexes per cm, i.e. about 5.88×10^8 complexes cm^{-1}.

Therefore per cm^2, one obtains $(5.88 \times 10^5)^2$ complexes cm^{-2}, i.e. 3.46×10^{11} complexes cm^{-2}.

Considering that one mole of complexes weights 2.79×10^6 g, and that one mole of complexes contains 6.02×10^{23} complexes, this results in $(3.46 \times 10^{11} / (6.02 \times 10^{23})) \cdot (2.79 \times 10^6)$ g cm^{-2}. This therefore yields 1400 ng cm^{-2} approximately.

5. Graphene growth by CVD. Transfer process. Assessment of graphene quality. Graphene was synthesized on Cu foils and transferred to SiO_2/Si wafers using procedures analogous to those in the literature.[3] In brief, large area graphene was synthesized on Cu foil 25 µm thick at 1000 °C by CVD of carbon using a highly diluted mixture of methane in hydrogen, in a furnace with about 4 cm inner diameter quartz tube and at ambient pressure. Before deposition, the Cu foil was annealed at 900 °C for 40 min under hydrogen flow in order to remove the metal oxide as well as enlarge the substrate grain size. During carbon deposition, the growth time was limited to a few minutes (~ 5 min). Following the growth, PMMA was spun on the graphene/Cu foil. The Cu foil was subsequently etched away using an iron chloride solution and then floated on the etchant solution, followed by repeated washing in deionized water. The floating

PMMA/graphene film was then transferred onto the SiO$_2$/Si substrate. Finally, the PMMA was dissolved away by immersing the PMMA/graphene film in an acetone bath at 50 $^\circ$C for 30 min.

After transfer to the SiO$_2$/Si wafer, the quality of the graphene film was checked with Raman spectroscopy under an excitation of 532 nm (Figure S4). The very sharp line (FWHM = 40 cm^{-1}) with one single Lorentzian profile of the 2D peak indicates that the graphene film forms a monolayer, while the small D peak indicates a low density of defects present.[4] This shows the high quality of our monolayer graphene film. The
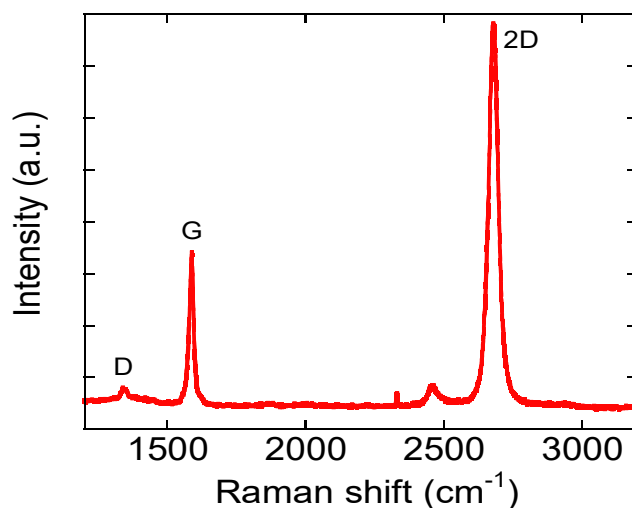

Figure S4: *Raman spectrum of our CVD graphene, indicating monolayer graphene and low defect density.*

FTIR indicates the presence of a range of functional groups (Figure S5) brought on the graphene sheet by the process of wet-transfer onto the final SiO$_2$ substrate: a broad band centred around 3434 cm^{-1}, corresponding to O-H stretching, and sharper spectral features at around 2920 and 2850, 2363, 1728, 1645, 1443, 1248 and 1034 cm^{-1}, assigned to asymmetric and symmetric C-H stretching, CO$_2$ stretching, C=O stretching, aromatic C=C and O-H bending, C-O stretching, epoxy C-O stretching, and alkoxy C-O stretching modes, respectively.[5-6] However, we note that the above spectroscopic features corresponding to polar groups are barely visible on top of the baseline of a representative raw FTIR spectrum, with un-extracted baseline, unlike the case of intentionally functionalized graphene shown in other works. The roughness analysis (based on AFM images analysed with the WSxM software)[7] shows increased roughness of the wet-transferred CVD graphene compared to exfoliated graphene (Figure S6).
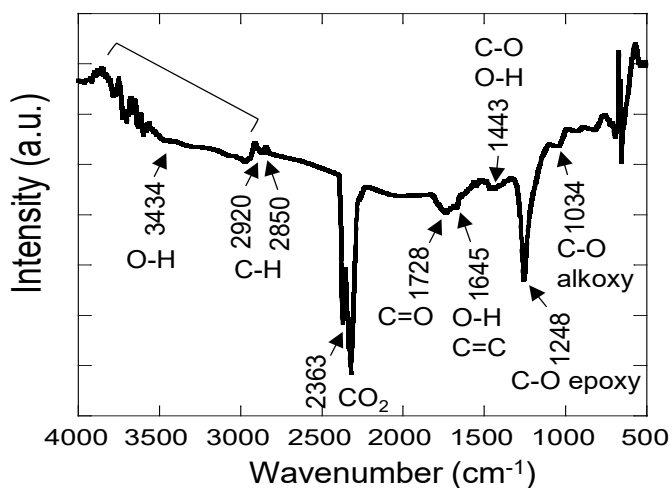

Figure S5: *FTIR spectra on wet-transferred CVD graphene, using PMMA as a supporting film.*
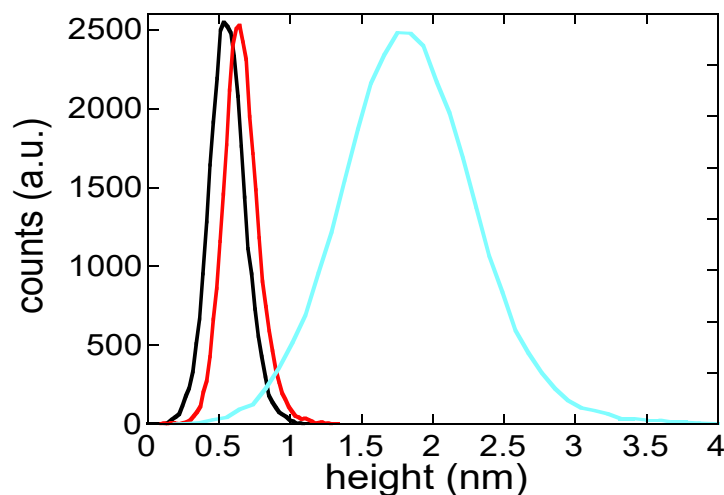
Figure S6: *Roughness profiles of three surfaces: SiO₂ (black), mechanically exfoliated monolayer graphene/SiO2 (red), and CVD monolayer graphene/SiO₂ (cyan) transferred using a wet-transfer process involving PMMA. Analysis was performed on 2x2 μm^2 areas using the "Roughness" feature of the WSxM software,[7] for SiO2 and large area, CVD graphene. For exfoliated graphene, the analysed area was the size of the flake.*

6. E2 monomer vs. E2 complex attachment on graphenic surfaces. E2 monomers were incubated on HOPG in similar conditions as described in Figure 1, main manuscript. Figure S7(a) shows that, unlike the E2 complexes (shown for comparison in Figure S7(c)), E2 monomers clustered together and possibly stacked on graphenic surfaces, creating an inhomogeneous protein layer with highly uneven height profile (Figure S7(b)). This demonstrates that E2 monomers failed to create monolayers, or layers with controlled thickness.
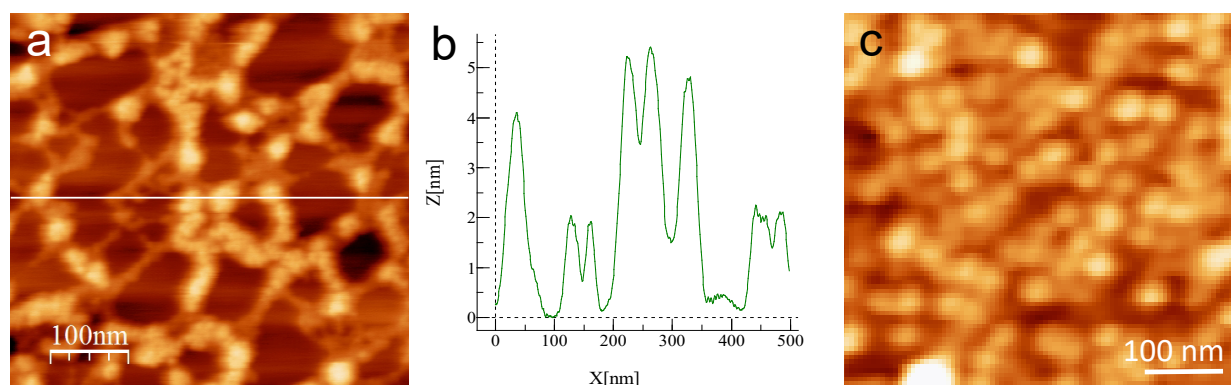

Figure S7: *Comparison between assembly/attachment of E2 monomers vs. E2 complexes on graphenic surfaces. (a) E2 monomers on HOPG, incubation for 40 s, from 0.1 mg/ml stock solution. (b) Topographic profile across the white line shown in (a). (c) E2 complexes on CVD graphene, part of Figure 2(b), main text.*

7. Self-assembly of E2 complexes on various graphenic surfaces. *Drying-mediated.* E2 complexes can form various types of self-assembled patterns, with the regimes of such assembly being controlled by the dynamics and the parameters (*e.g.* complex concentration and temperature) of the drying process.[8-9] Examples of such assembly are shown in Figure S8: these were obtained from incubation of E2 complex

solutions of 0.1 mg/ml concentration for varying incubation times. As a result of heterogeneous evaporation[10] (where E2 complexes are trapped in the liquid wetting the surface, between solvent on one side of the drying front and air on the other, and pushed by the receding drying front), one can develop highly ramified networks (a-b), or "cellular" patterns, as in (c-d). Following homogeneous solvent evaporation, islands of complexes can grow larger by coarsening as the domain boundaries remain fluxional and wetted by the solvent on all sides during drying;[8] this results in (e) large islands and coalescence, with "cracking" being characteristic of monolayer formation.[11] Individual E2 complexes are clearly distinguishable in all cases, within the compact areas. We stress that we are using the drying-mediated assembly to demonstrate the ability of the E2 complexes to move on various graphenic surfaces, as opposed to presenting well-defined recipes for obtaining one type of pattern or the other.
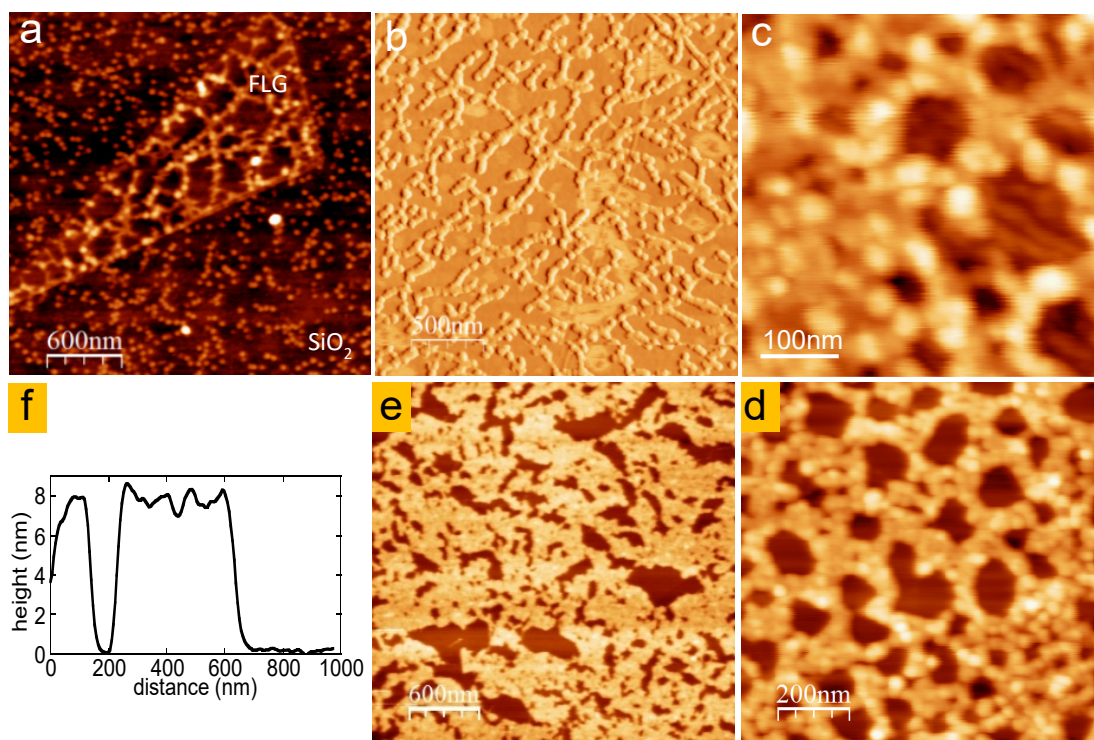

Figure S8: *Drying-mediated, self-assembly E2 complex patterns on (a,b) mechanically exfoliated FLG supported by SiO$_2$ substrate, (c) CVD graphene, and (e,d) HOPG. (f) Topographic profile taken across the protein islands formed on HOPG in (e). All images were obtained using tapping mode in air, in an attractive regime (resulting in no compression), see below; all are topographic images except (b) which is a phase image, for clarity. (a) also demonstrates the lack of mobility of the E2 complexes on the SiO$_2$ regions that surround the FLG flake. Typical scanning conditions: cantilevers with a spring constant of ~ 2 N/m, resonance frequencies of ~ 73 kHz, quality factor Q ~ 160, free oscillation amplitudes of ~ 5 nm, and 'measured amplitude-to-free amplitude ratios' (i.e. scanning set-point) of 80%.*

We also note from Figure S8 (a) that E2 complexes are immobile and do not self-assemble in patterns on the hydrophilic surface of the SiO$_2$ substrate surrounding the graphene flake in that image, despite doing so on the exfoliated graphene flake (FLG) in the same image (as well as in any other similar cases observed). This correlates with the lower apparent height of the E2 complexes measured on such SiO$_2$ surfaces in both Figures S8(a) and S11(c), altogether suggesting a stronger interaction of the E2 complexes with these

surfaces than with the graphene-like ones, as discussed in the main text. See also discussion of Figure S9 for comparison of E2 corrected heights on these surfaces.

Figure S8(f) also shows that under similar scanning conditions as those used for Figure 2 (main text) the apparent height of the assembled E2 islands is ~ 8-9 nm, consistent with the measurements on individual complexes shown in the main text.

Assembly from liquid phase. Figure S9 shows the E2 complexes being assembled directly from liquid phase onto HOPG, from E2 complex solution of 0.1 mg/ml concentration, after 5 minutes of incubation time. Subsequent scanning with the same speed (~ 3 Hz/line) over a smaller area (see inset), resulted in the removal of the proteins from that surface, indicating a low E2 complex - HOPG interaction.
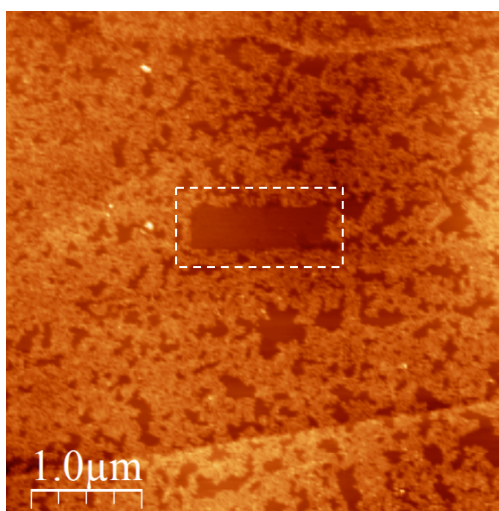

Figure S9: Assembly from liquid phase on HOPG, and removal of E2 complexes through fast scanning (~ 3Hz/line) over a small area (framed). AFM image obtained by scanning in liquid (on a Cypher microscope), using stiff, short cantilevers (BioLever Fast, 9µm, 0.1 N/m, 1.5 MHz from Olympus) to ensure small oscillation amplitudes, and without complex fixation.

8. Morphology of E2 complexes on various surfaces. Real vs. apparent height. It is well known that determining the real height of proteins with AFM is challenging.[12] In general, forces need to be minimised to avoid compression and deformation of such soft structures, and for this reason imaging in liquid is preferable. However, this requires protein fixation *via* specific protocols,[13] as well as working at isoelectric point in order to minimise electrostatic forces induced by charges residing on the protein surface while in liquid.[14] In general, protein fixation induces crosslinking of the end groups of protein molecules, allowing AFM imaging in liquid without the proteins being moved laterally by the AFM tip. We attempted two fixation protocols of E2 on graphene and HOPG: (i) by allowing the E2 complexes to dry on the surface (after washing with buffer and DI water) and subsequent application of 1% glutaraldehyde for 5 minutes, or (ii) by incubation from a drop of liquid, rinsing with PBS, and then application, while the surface was still wet, of 1% glutaraldehyde for 5 minutes. In both cases, the surfaces were subsequently washed with PBS and alcohol and not allowed to dry. Unfortunately, fixation was unsuccessful when the E2 complexes were not allowed to dry on surfaces prior to application of glutaraldehyde; while when the proteins were dried on surfaces prior to fixation, non-uniform aggregates of complexes formed instead of monolayers after subsequent immersion in PBS.

For this reason, we resorted to the measurement and comparison of "apparent" heights of the E2 complexes from tapping mode AFM in air, on samples where the complexes were attached on various surfaces - graphenic, i.e. hydrophobic, or SiO2 and sapphire, i.e. hydrophilic - by filter drying, as in Figure 2 (main text) and Figures S8 and S11 here; then the "apparent" heights were corrected through analysis of spectroscopic curves performed over the bare substrates and the substrate-supported E2 to yield real height profiles. This required carefully chosen scanning conditions: imaging was performed under average forces of attractive character (characterized by an experimentally measured phase > 90°),[12] where the peak dynamic force was maintained in the attractive regime (see simulation below); in contrast, repulsive dynamic forces (characterised by a measured phase < 90°) are compressive in nature and of one or two orders of magnitude larger (i.e. in the nN range and beyond), therefore inducing strong compression and destruction of the proteins.[12] Using our experimental imaging conditions (i.e. cantilevers with a spring constant of ~ 2 N/m, resonance frequencies of ~ 73 kHz, quality factor Q ~ 160, typical free oscillation amplitudes of ~ 5 nm, and set-points, i.e. measured amplitude-to-free amplitude ratios of 70-85%) we fully characterized the imaging regime in which our data were taken, by simulating spectroscopic distance-dependence measurements for oscillation amplitude, phase, peak dynamic force, and contact time, respectively; for both graphenic surfaces (such as graphene and HOPG), and SiO2 or sapphire. Such simulations clarified the differences between the "real" and "apparent" heights for the two types of surfaces (hydrophobic *vs* hydrophilic), allowing us to correct the experimentally measured ("apparent") heights, and to correlate the corrected E2 heights with other information we obtained regarding the strength of the interaction between E2 and the respective substrates. The simulation of the spectroscopic data used a dynamic model for the oscillating cantilever similar to that described by Garcia et al.[15] This implied the consideration of equations (S.1) describing the tip motion resulting from the driven cantilever being subjected to various types of interaction forces (that sum to the total force F_{total}) during its oscillation:

$$\frac{d^2z}{dt^2} + \frac{\omega_0}{Q}\left(\frac{dz}{dt} - \frac{d\zeta}{dt}\right) + \omega_0^2\left(z - \zeta\right) = \frac{\omega_0^2}{k_c}F_{total} \qquad (S.1)$$

$$\zeta = \frac{A_0}{Q}\cos\left(\omega_0 t\right)$$

where $\omega_0 = 2\pi f_0$ and f_0 is the driving frequency of the cantilever, Q is its quality factor (here ~ 160), k_c its spring constant (~ 2 Nm⁻¹), and A_0 is the driving amplitude. The forces acting on the cantilever and included in F_{total} were a van der Waals interaction, characterized by a Hamaker constant H, a short range Lennard-Jones interaction, and an adhesion force (see below equations (S.2)) when intermittent contact develops:[15]

$$F_{ad}\left(d\right) = -\frac{H \cdot R}{6a_0^2} + \frac{4}{3}E^*\sqrt{R}\left(a_0 - d\right)^{3/2}$$

$$\qquad (S.2)$$

$$\frac{1}{E^*} = \frac{\left(1 - v_t^2\right)}{E_t} + \frac{\left(1 - v_s^2\right)}{E_s}$$

Here F_{ad} is the adhesion force, d is the distance to the surface, R is the tip radius, E_x and ν_x are the tip (sample) elastic modulus and Poisson coefficient, respectively, while a_0 is an intermolecular distance, taken here as 3.7 Å.[15] We then considered numerical values[15] for the elastic modulus E, the Hamaker constant H, and the Poisson coefficient ν for (i) HOPG (10 GPa, 60×10^{-20} J, and 0.3, respectively),[16] (ii) a bio-surface of intermediate compliance, like polystyrene (1.2 GPa, 7.1×10^{-20} J, and 0.3, respectively), and (iii) another bio-surface of high compliance, like polyehylene (0.087 GPa, 6.6×10^{-20} J, and 0.3, respectively).[15] We considered the E2 complexes to be between cases (ii) and (iii) in their mechanical properties, though these mechanical properties hardly affect the forces in the attractive regime when no intermittent contact takes place with the protein surface, as confirmed by the simulations. For the silicon tip we considered E, H and ν of 130 GPa, 6.4×10^{-20} J, and 0.3, respectively.[15]

Figure S10 (a, c and e) shows the resulting amplitude-distance, phase-distance and peak force-distance curves when an E2 complex is positioned above the HOPG surface. These curves show that the imaging regime we operated in is characterized by an overall average force that is attractive in nature (i.e. phase is > $90°$) and of very low magnitude, so that there is zero compression of the E2 complex during imaging. Further, by considering a set-point of ~ 80% on the amplitude-distance curve from Figure S10(a), we determined that the tip lies at different distances to the surface when above the HOPG or graphene substrate than above the E2 complex: this results in the "apparent" (measured) height of the E2 complex being smaller than the real height. Figure S10(a) shows that Δh ~ 2nm needs to be added to the "apparent" height of 8-9 nm (determined from Figure 2, main text) of the E2 complexes, resulting in a real height of the E2 complexes on graphenic surfaces of ~ 10-11 nm. These values are to be compared to the projected diameter of the E2 complexes as determined from TEM (Figure 3(a), main text), of ~ 16-17 nm. Hence, the comparison reveals that the E2 complexes are compressed by about 22-28% by the interaction with the graphenic surfaces.

The situation is much more dramatic when the substrate is SiO_2 (characterized by E, H and ν of 70 GPa, 6.4×10^{-20} J, and 0.3, respectively) or sapphire: analogous simulations show that in this case there is no correction to be added to the measured height, of ~ 4 nm, of the E2 complexes. This is because the tip hovers essentially at the same distance above the bare SiO_2 surface as above the E2 complex (see Figure S10 (b)): this is the result of the Hamaker constants for proteins (equated here as soft matter) and SiO_2 (or sapphire) being not that dissimilar, but vastly dissimilar compared to conductive surfaces such as HOPG or graphene. Hence, the resulting real height of ~ 4 nm of the E2 complexes on the hydrophilic SiO_2 or sapphire surfaces show that E2 complexes suffer a much larger compression on such surfaces than when immobilised on the graphenic substrates (where a corrected height of the E2 complexes of ~ 10-11 nm was obtained). This indicates a stronger interaction of the E2 complexes with SiO_2 (or sapphire), also consistent with the lack of mobility of the complexes on SiO_2 during the drying-mediated assembly experiments (as shown by Figure S8 (a)).

The simulations also confirmed what was observed experimentally, that with these low oscillation amplitudes the dynamic forces between the tip and E2 are of attractive nature, meaning that no additional compression is exerted by the AFM tip. Only above the hard, bare SiO_2 surface does the force change character and become repulsive (shown by the phase jump from above to below $90°$, Figure S10 (d)) and in the nN range (Figure S10 (f)), when decreasing tip-to-surface distances.
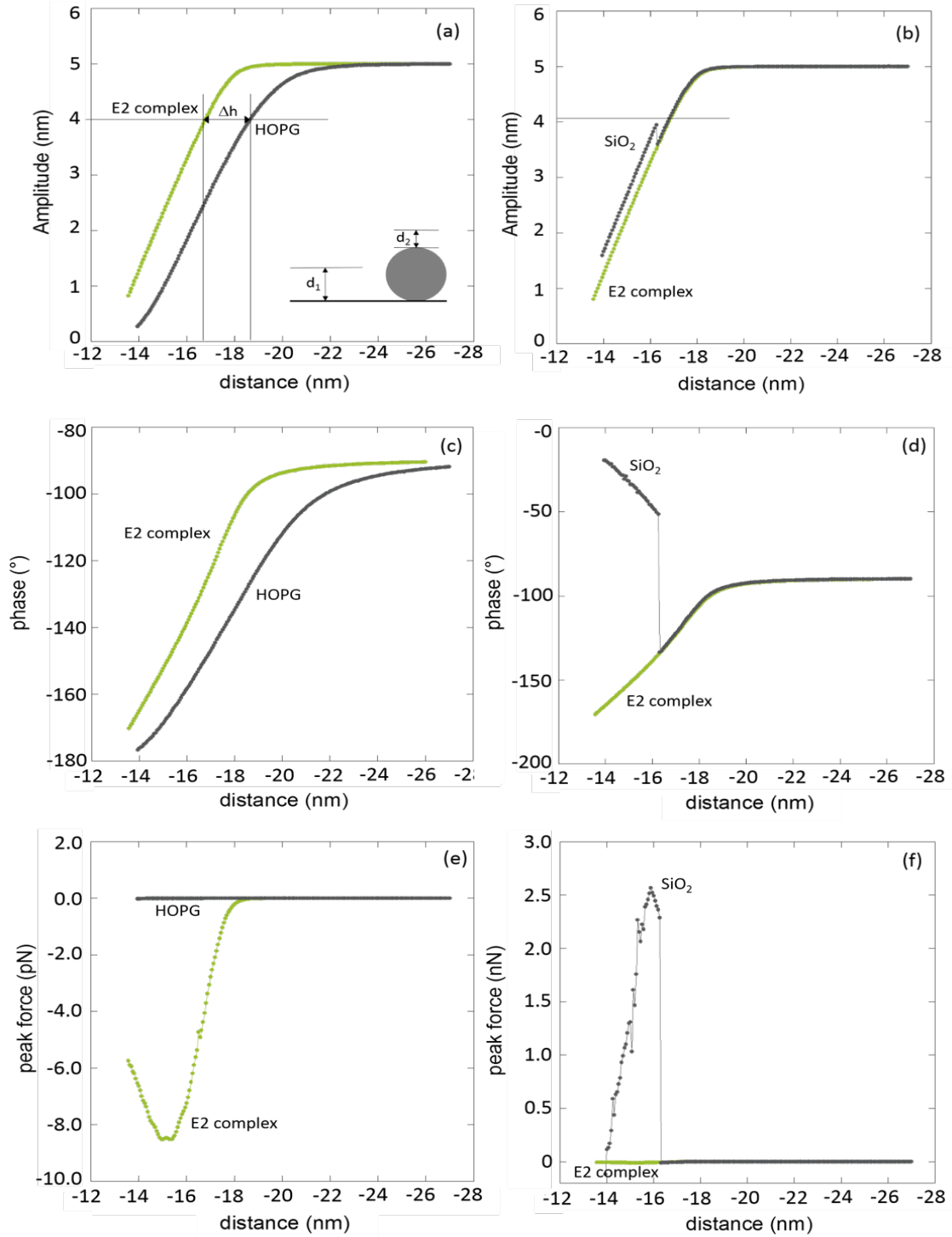
Figure S10: *Simulated distance-dependent spectroscopic measurements, for oscillation conditions matching the experimental conditions. (a),(c),(e) amplitude-distance, phase-distance, and peak-force-distance curves, respectively, taken above E2 on a graphenic substrate (green), and above the bare HOPG substrate (dark grey). (b), (d), (f) Similar spectroscopic curves taken above E2 on SiO_2 (green), and above the bare SiO_2 substrate (dark grey). Scanning conditions indicated by the straight lines in (a) and (b) (corresponding to a set point 'measured amplitude-to-free amplitude' of ~ 80%), led to a $\Delta h = 2$ nm correction to be added to the measured height of E2 on HOPG or graphene. This correction is the result of the AFM tip positioning itself at*

a lower distance above E2 than above HOPG or graphene during scanning (when a constant amplitude must be maintained), as shown in the inset of (a). No correction is needed when E2 is attached to SiO₂ as shown by the analysis of (b). In (e) and (f), force character is attractive for negative values, and repulsive for positive values.
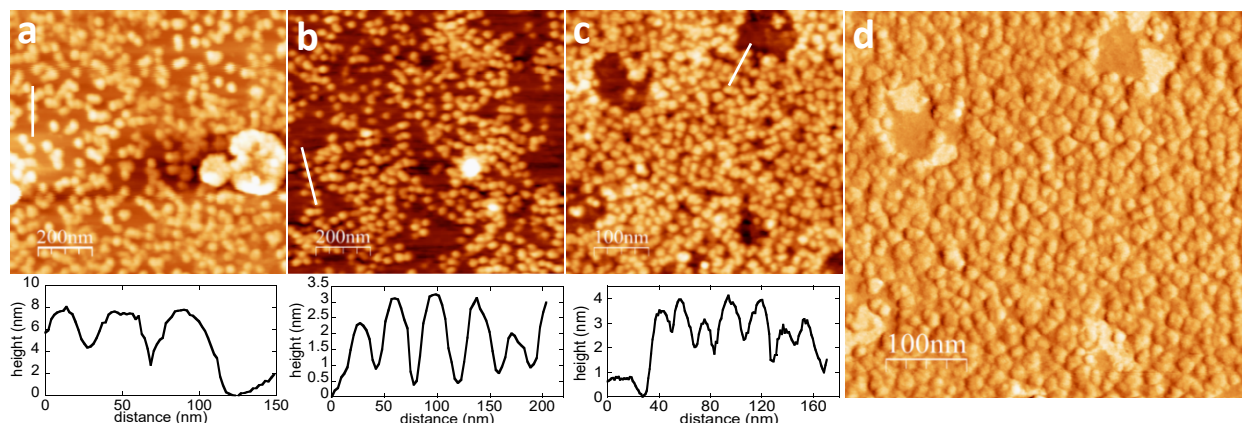

Figure S11: *Tapping mode in air in an attractive regime, in conditions similar to those described in text (cantilevers with a spring constant of ~ 2 N/m, resonance frequencies of ~ 73 kHz, quality factor Q ~ 160, typical free oscillation amplitudes of ~ 5nm, and measured amplitude-to-free amplitude ratios of 80%) clearly showing regular, individual structures identified as the E2 complexes. (a), (b) and (c) show the complexes on HOPG functionalized with a linker used to prevent protein collapse, hydrophilic sapphire, and SiO₂/Si wafer surface, respectively; (d) is the phase image corresponding to the topographic image in (c), resolving the central depression of individual E2 complexes, similarly as in Figure 3, main text. Insets: topographic profiles, showing the resulting apparent heights for each case.*

9. FET control experiments assessing E2 and E1 attachment. To unambiguously identify changes in FET operation that are due solely to E1 attachment to the E2-graphene platform, and through this to obtain evidence of the E1 attachment, several control experiments were performed. We first needed to assess the starting doping state of the CVD graphene film, and then understand the effects of exposure to PBS (via which the double-layer used for electrochemical gating forms) (Figure S12), of the E2 layer formation on the graphene surface (Figure S13), and finally, that of E1 build-up onto E2-graphene (Figure 4, main text). This was achieved by monitoring the changes in the transconductance curve, i.e. the source-drain characteristic as a function of gate voltage, and the shift in the position of its Dirac point (alternatively referred to as the charge neutrality point, CNP) relative to the gate voltage.

Transconductance as a function of buffer ionic strength (Figure S12). CVD graphene was found to be p-doped (i.e. the Dirac point is located at positive gate voltages V_g) after the transfer process (using PMMA and FeCl₃) to the SiO₂ substrate, in agreement with previous work,[17-21] while addition of PBS of increasing ionic strength as a gate electrolyte made the Dirac point shift in the opposite direction with gate voltage (Figure S12(a)), making the graphene less p-doped, also in agreement with previous findings.[22] The shift of the Dirac point towards lower gate voltages follows a linear trend with increasing the buffer concentration (Figure S12(b)). This neutralizing of graphene is a reversible process as rinsing the device with DI water leads to the complete recovery of the initial Dirac point position in the concentration series (dashed line in Figure S12(a)).
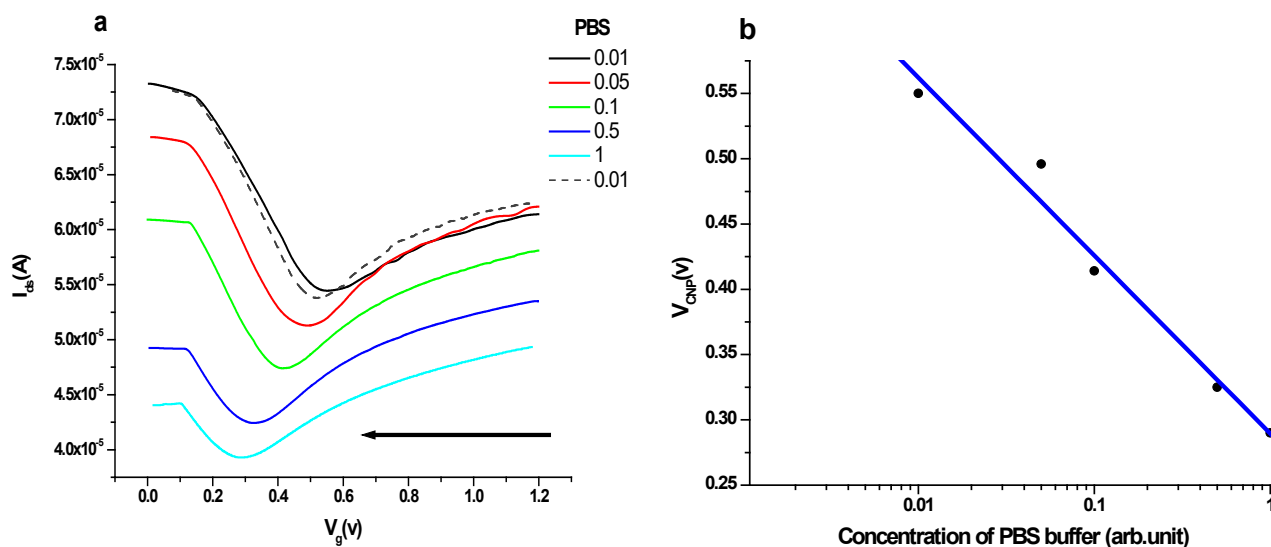
Figure S12: *(a) Typical variations of transconductance curves obtained with increasing the ionic strength of the PBS (from 0.01× to 1× dilution factors, as indicated in legend). 40 μl of PBS were placed in a PDMS reservoir defining an active graphene area of ~ 12 mm², and left to stabilize for 30 minutes before measuring; between each new concentration, the graphene surface was rinsed thoroughly by pipetting DI water. In a final step, the graphene surface was rinsed with DI water, and buffer solution of the lowest concentration was added (dashed line). Arrow indicates the direction of the Dirac point shift with increasing PBS concentration. (b) The position of the Dirac point (V_{CNP}) decreases linearly with increasing the concentration of PBS solution.*

Transconductance shift during E2 layer build-up (Figure S13). 20 μl drops of solution of varying E2 concentration (from 0.01 mg/mM to 1 mg/mM) were left to incubate for 10 minutes each over the graphene surface, after which the surface was washed by pipetting fresh PBS buffer to remove un-bound E2 and residual salt, while measurements were taken after further stabilization for 10 min in full strength, pure PBS electrolyte – allowing to probe the E2-graphene interface. The final E2 concentration of 1 mg/ml is ten times higher than the one used for incubation in the AFM and electrochemistry measurements. Figure S13 shows the resulting transconductance curves before and after each of these incubations. The Dirac point is seen to shift towards larger, positive gate voltages, i.e. *opposite* to the effect of the PBS, demonstrating a trend that is clearly related to the attachment of the E2 complexes onto graphene. This trend has been verified on n=3 independent experiments. The shift of the Dirac point suggests further p-doping of graphene. We attribute this shift to cysteine residues, known to be located on the binding and catalytic domains of the E2 monomers:[23] cysteine amino acids can p-dope graphene[24] due to the presence of SH groups able to withdraw electrons from graphene.
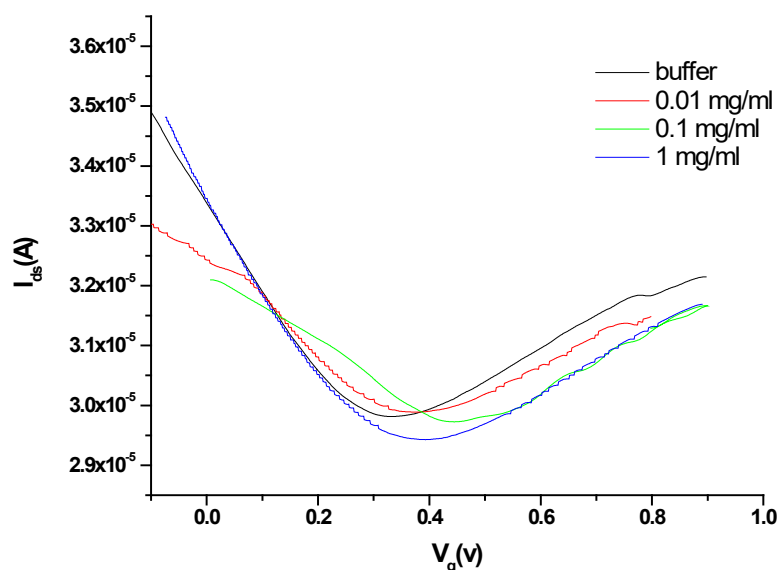
Figure S13: *Transconductance curves after successive incubations with increasing concentrations of E2 in PBS. Measurement procedure as described in text.*

Transconductance shift with E1 build-up on E2-graphene. Discussion of behaviour from Figure 4, main text. This figure shows the evolution of the transconductance characteristics once the E2 layer has been established on the graphene surface. E1 of various concentrations was then incubated for 10 minutes each (as described in Methods), followed by rinsing with PBS to remove any unbound E1, and further addition of 40 µl fresh diluted PBS as electrolyte (Debye length $\sim$ 3.5 nm) for the transconductance measurements. The result of the E1 incubation leads to a different trend than those observed through exposure to PBS (Figure S12), or during E2 attachment to the graphene surface (Figure S13): the transconductance curves widen upon increasing the concentration of E1 to which graphene has been exposed, accompanied also by a shift of the Dirac point towards larger gate voltages. The rightwards shift of the Dirac point completely rules out any potential artefact due to salt build-up from PBS on the surface, as any such effects should be included in a leftwards shift of the Dirac point (Figure S12); moreover, any stabilization in PBS has long taken effect through previous exposures to PBS. As the AFM images show a height of around 10-11 nm measured at the top of the complexes, which is larger than the Debye length (though this is not the case for interfacial regions between adjacent complexes where the layer thickness is at its lowest), we submit that the changes in the transconductance curves are mainly due to changes in the dielectric constant of the electrical double layer at the solid liquid interface leading to a change in the gate efficiency of the electrolyte rather than a charge transfer effect due to E1. A similar behaviour was also observed by Chen *et al*.[25]

10. Supporting and control electrochemistry experiments.

Cyclic voltammetry and chronoamperometry of E1 bound to E2-graphene. Cyclic voltammetry. Figure S14 shows three sets of cyclic voltammetry (CV) curves corresponding to three DCPIP mediator concentrations, and spanning a wide range of substrate concentration. The set from Figure S14 (a), obtained at 10 µM DCPIP, corresponds to Figure 4(d) in the main text; while the set from Figure S14 (c), at 100 µM DCPIP, provided the CV-derived kinetics data used in Figure 4(e) to be compared with chronoamperomtric

data obtained at same DCPIP concentration. The three sets of data show that bioelectrocatalysis takes place in all cases, and with similar overall behaviour as a function of substrate concentration.
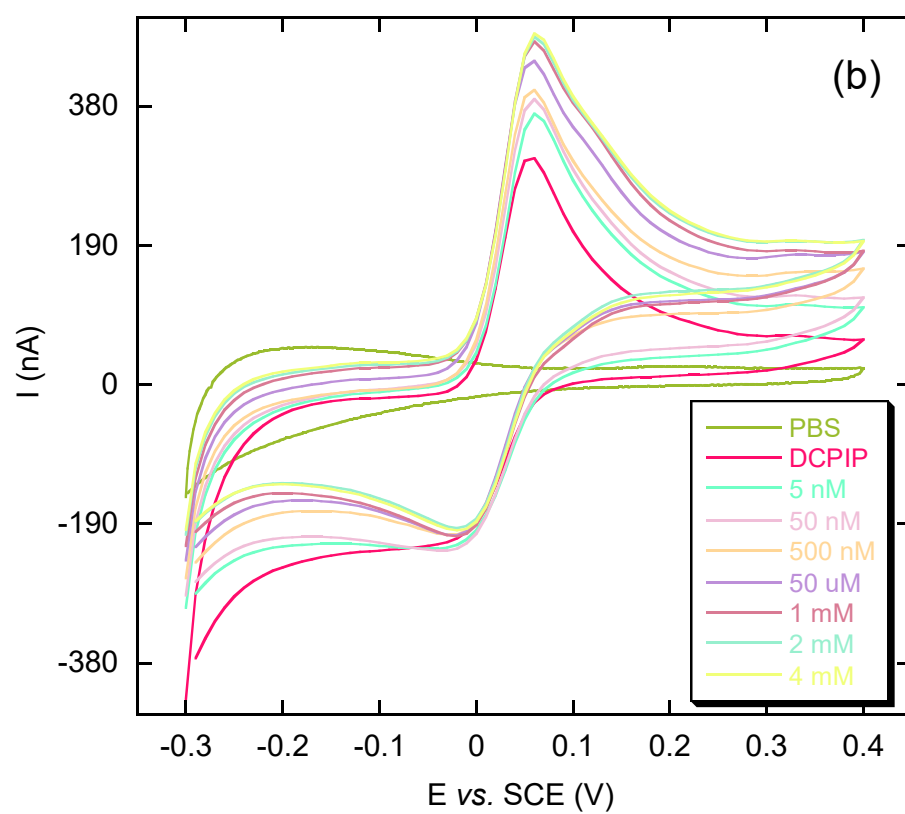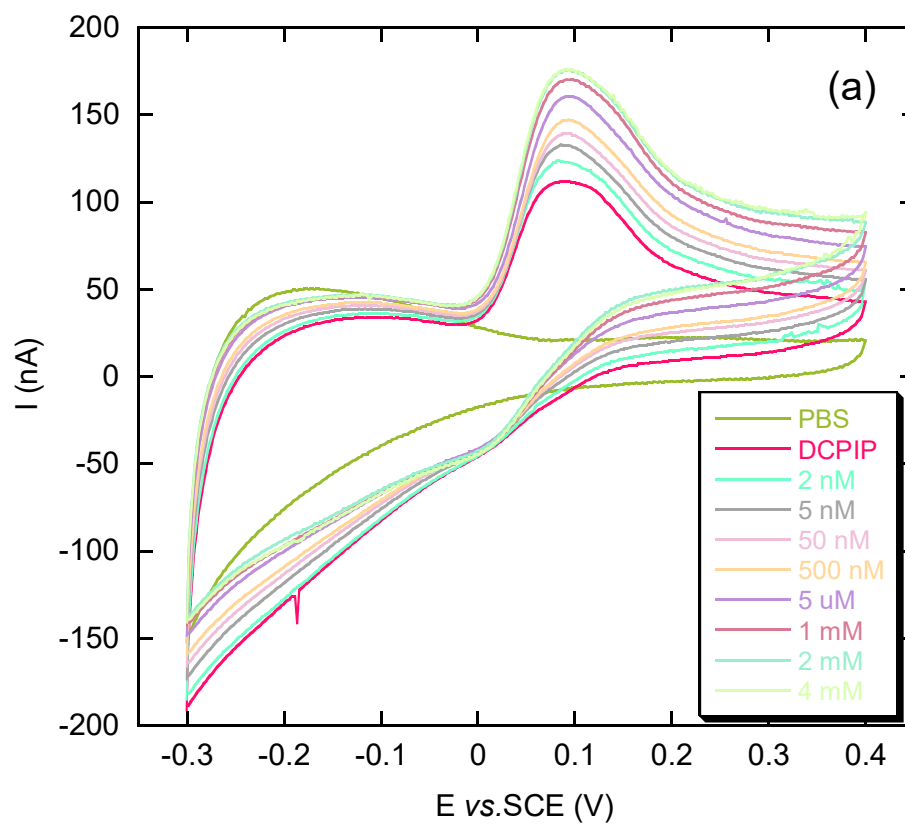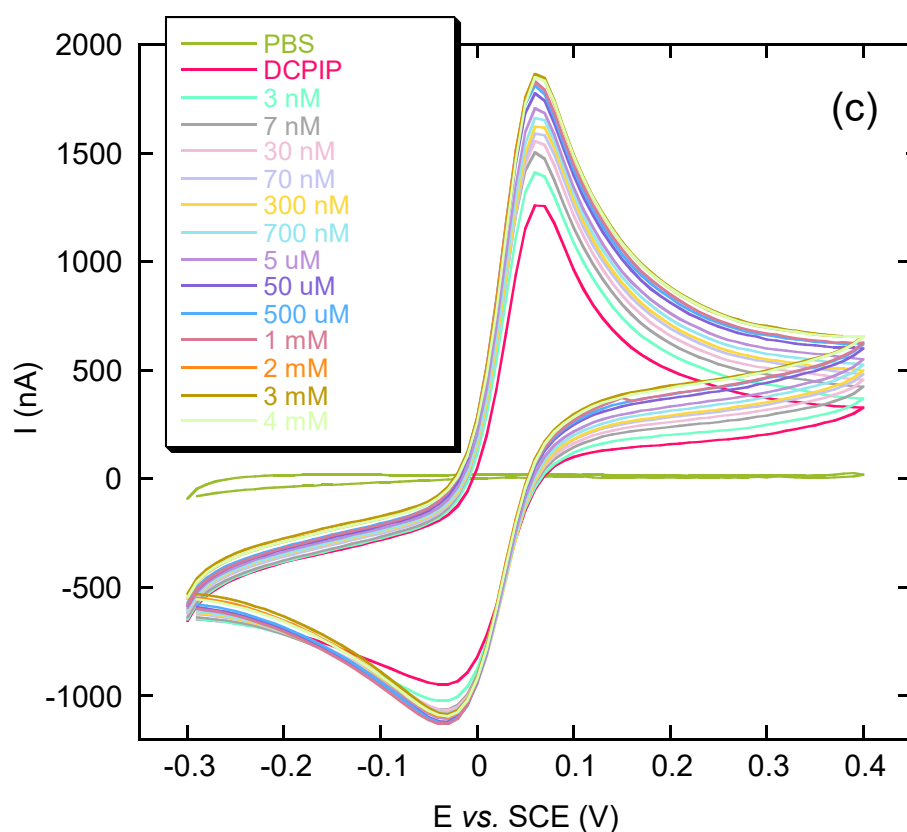
Figure S14: *Cyclic voltammograms of E1-E2-graphene for a wide range of substrate concentrations and for different mediator (DCPIP) concentrations: (a) 10 μM DCPIP, corresponding to Figure 4(d) main text; (b) 30 μM DCPIP; and (c) 100 μM DCPIP. Curves corresponding to PBS only (olive), and after addition of DCPIP mediator, but without substrate (red) are also shown. Scan rate was 0.03 V s^{-1}, while incubation conditions and other details as in Experimental Section.*

Chronoamperometry details and raw data. As Ag was used as a reference electrode instead of SCE (used in the CV experiments) it was necessary to perform cyclic voltammetry to determine how the redox potential of the reaction vs. the Ag electrode shifted compared to SCE. Figure S15 shows there was no significant change in the peak position induced by DCPIP compared to voltammograms using SCE, shown in Figure S14; a potential value of 0.25 V was then chosen for the amperometric experiments.

Figure S16 shows the raw chronoamperometric data from which the E1 kinetics from Figure 4(e), main text, was determined.
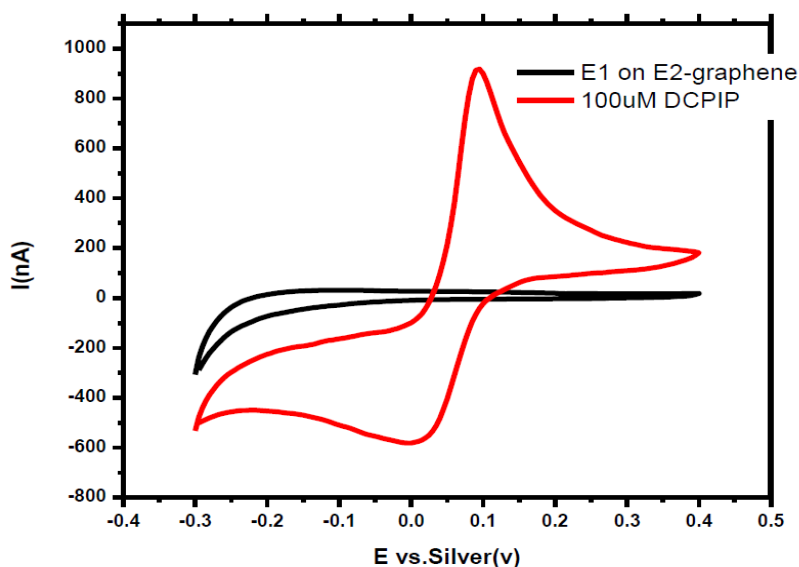
Figure S15: *Cyclic voltammogram of E1-E2-graphene in PBS in presence of 100 μM DCPIP (red curve) obtained by using an Ag reference electrode. The black curve represents the response of E1-E2-graphene in the absence of the DCPIP mediator. Reaction volume was 10 ml.*
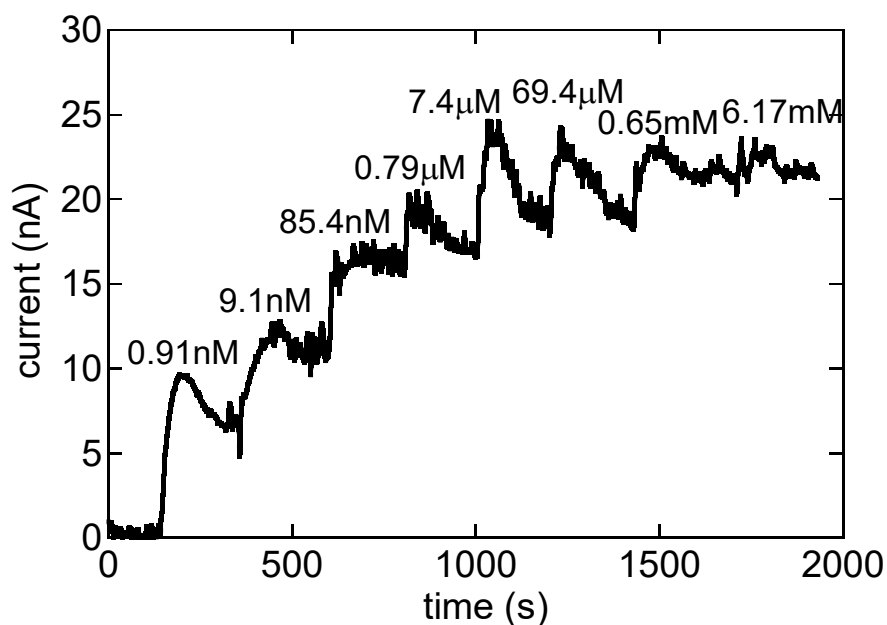

Figure S16: *Raw chronoamperometry data from an experiment performed in a drop of liquid covering the graphene surface with applied potential of 0.25 V vs. Ag/AgCl. Current was measured after additions of 2 μl substrate of various final concentrations (indicated) to 20 μl drop of buffer with 100 μM DCPIP.*

Fits of kinetics data from CV and amperometry. Figure S17 uses the chronoamperometric and CV-derived kinetics data from Figure 4(e) and provides comparisons between fits with a non-Michaelis Menten enzyme kinetics law (of the type $I = A/(1+(B/[S])^n$, with $n < 1$) and Michaelis-Menten kinetics (of the type $I = A/(1+(K_m/[S]))$) applied only to the region of data at high substrate concentration. *[S]* is the substrate concentration. Table S1 shows values of the respective parameters obtained as a result of these fits.

The error bars in the CV-derived data encompass variations in the current across five successive CV measurements at a given substrate concentration. In general, current values settled and became largely reproducible from one CV cycle to another after the second cycle.

Table S1: Parameters derived from fitted chronoamperometric and CV-derived kinetics data

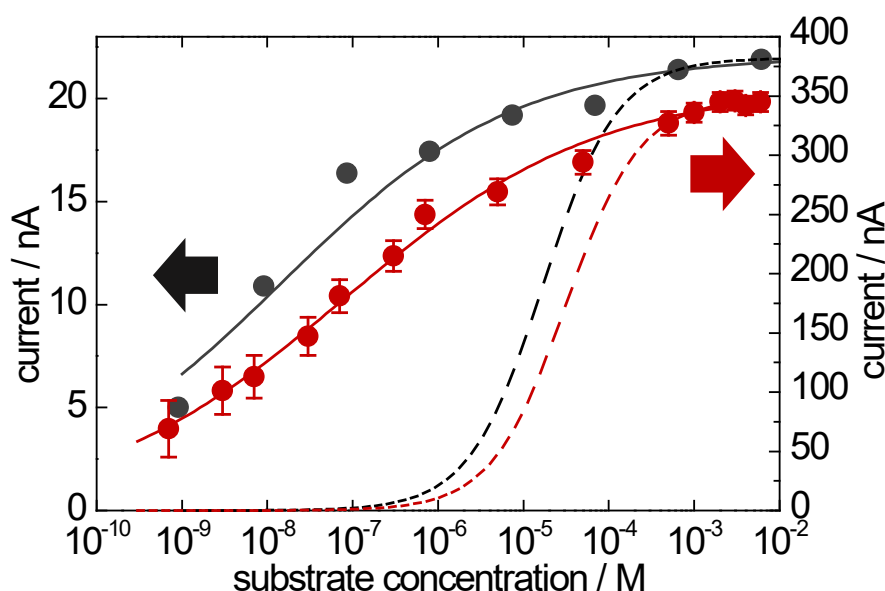|	$I = A/(1+(B/[S])^n$ non-Michaelis Menten		$I = A/(1+(K_m/[S])$ Michaelis-Menten (above 10^{-5} M)
	B (M)	n	K_m (M)
Amperometry	$1.45 \ 10^{-8} \pm 7.2 \ 10^{-9}$	0.31 ± 0.05	$1.7 \ 10^{-5}$
C-V	$7.45 \ 10^{-8} \pm 1.3 \ 10^{-8}$	0.3 ± 0.016	$3.1 \ 10^{-5}$

Figure S17: *The E1 kinetics data from Figure 4(e) main text could be fitted over the whole substrate concentration range with a non-Michaelis-Menten law; fits shown with continuous lines of data are from the decayed values of amperometric current steps (at 0.25 V vs. silver electrode) (black), and from the anodic current peak (at 80 mV vs. SCE) of the CV curves (red). Fits with Michaelis-Menten laws of the data at the highest concentrations, above 10^{-5} M, are shown with dashed lines. 100 μM DCPIP concentration was used. A linear-logarithmic data display was used.*

Control experiments: bare graphene, E2-graphene, E1-BSA-graphene. Figure S18 (a) shows a set of cyclic voltammograms corresponding to bare graphene, tested successively in the presence of PBS only, followed by addition of DCPIP, and then E1 substrate of varying concentrations. Figure S18 s(b) shows E2-graphene, *without E1*, subjected to the same test sequence: PBS only on unfunctionalized graphene (black), then PBS only of E2-functionalized graphene (olive), followed by added DCPIP (red), and followed by increasing concentrations of E1 substrate. In the E2-graphene case, for a comprehensive control test, the same graphene electrode was tested with PBS both before and after incubation with E2. No increased

catalytic activity was detected, at least within about 5% of the value corresponding to the DCPIP-related current, over the full substrate concentration range used.
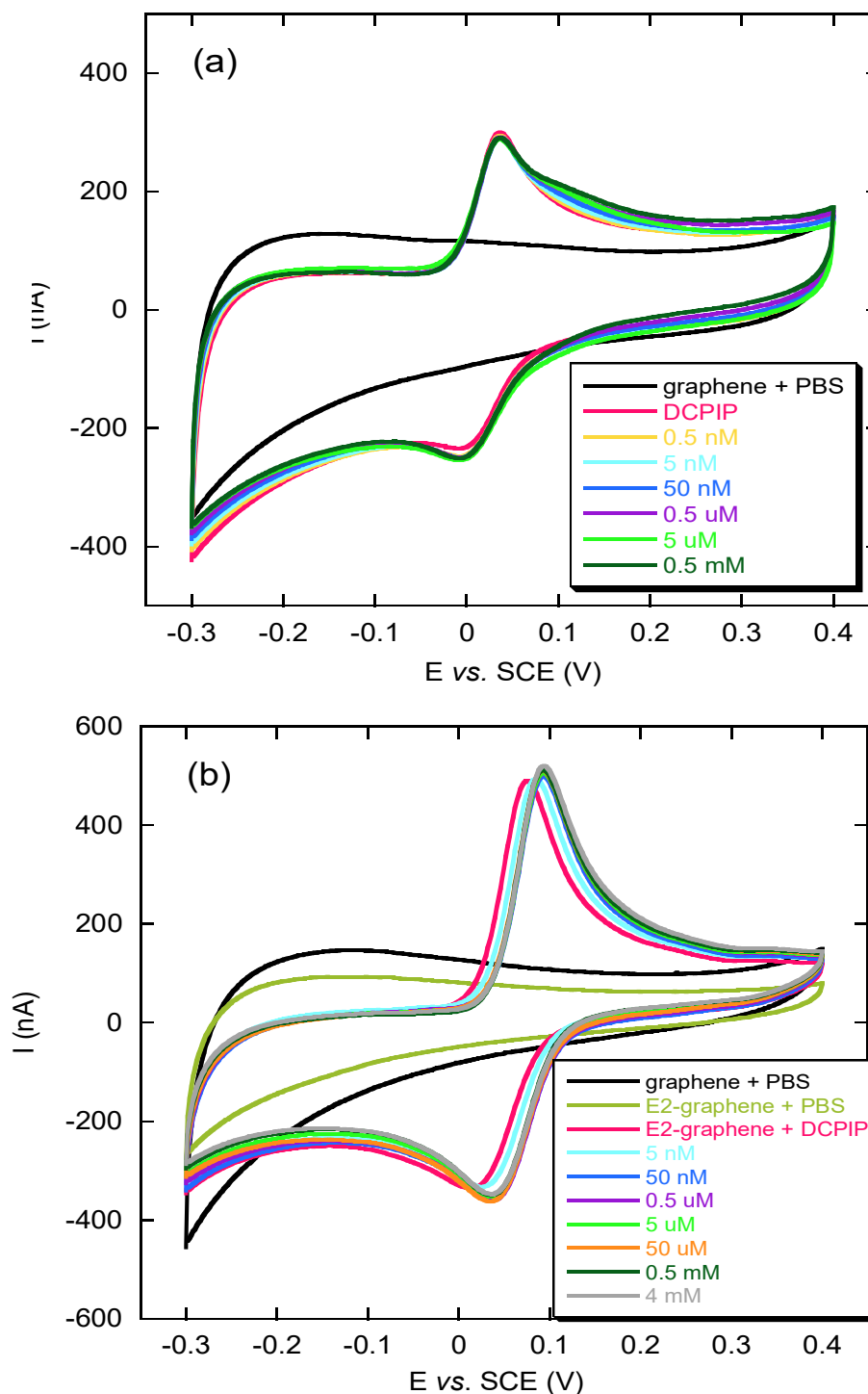

Figure S18: *(a) Cyclic voltammograms of bare graphene in PBS (black), after 10 μM DCPIP addition (red), followed by additions of E1 substrate of increasing concentrations. (b) Cyclic voltammograms of bare graphene in PBS (black); and after E2 incubation, with successively added PBS (olive), 30 μM DCPIP (red), followed by additions of E1 substrate of increasing concentrations. Volume of reaction was 10 ml, DCPIP and substrate concentration shown are after dilution in reaction volume. No E1 is present in these tests.*

Figure S19 shows the lack of activity of E1 when incubated on BSA-graphene, and following a similar test sequence: PBS only with E1-BSA-graphene, then with added DCPIP, and then followed by sequential additions of substrate. Sample preparation was identical to E1-E2-graphene in terms of concentrations of stock solutions and incubation times.
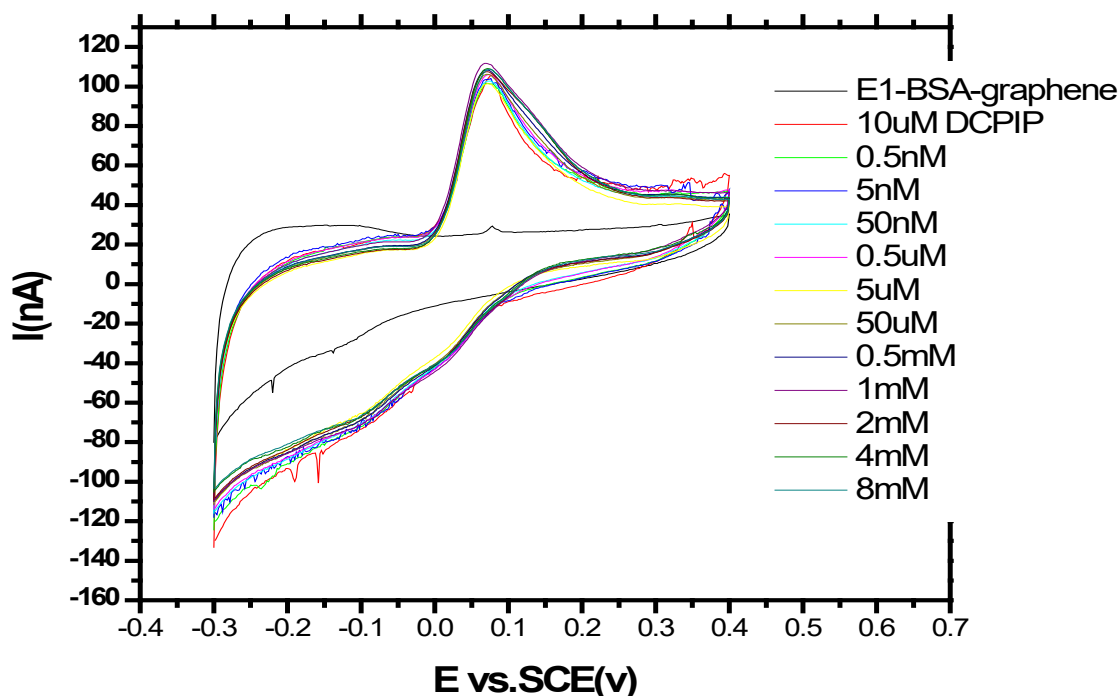

Figure S19: *Cyclic voltammograms of E1-BSA-graphene, in PBS (black), after addition of 10 μM DCPIP (red), followed by substrate of increasing concentrations. Scan rate was 0.03 V s^{-1}.*

DCPIP redox processes at CVD graphene. Figure S20 (a) shows a set of cyclic voltammograms representative for our PMMA-transferred CVD electrodes with DCPIP as mediator and for varying scan rates. As an example, at the lowest scan rate, ΔE_p between the reduction and oxidation peaks was found to be ~ 29 mV; this correponds to 0.59 mV/n, with n=2 electrons exchanged[26-27] in the reaction involving DCPIP. The voltammogram's anodic peak current varied as a power law with the scan rate, with an exponent of about 0.55 (Figure S20 (b)), suggesting that the DCPIP redox process on CVD graphene electrodes is predominantly diffusion controlled (this is the case for a process varying with the square root of the scanning speed).[26-27] An approximation for the effective area of the graphene electrode can then be obtained based on the Randles-Sevcik equation:[26-27]

$$I_p = 0.4463 \cdot (n \cdot F)^{3/2} A \cdot \left(\frac{D}{RT} \right)^{1/2} \cdot v^{1/2} \cdot C^* \tag{S.3}$$

where I_p is the maximum current of the voltammogram (in Amps), A is the electrode active area (in cm^2), F, the Faraday constant (in C mol^{-1}), D is the diffusion coefficient (in cm^2/s), C^* is the concentration of mediator (in mol/cm^3), n is the number of electrons involved in the reaction, and v is the scan rate (in V/s). Here values corresponding to DCPIP, C^* = 10 μM, D = 7.7×10^{-6} cm^2/s,[28] and considering n = 2 (as above), yielded an

effective area of 7.5 ± 0.5 mm^2 vs. a geometric area of 10.5 mm^2 in this particular case. A ratio of A/A$_{geometric}$ = 72 ± 5% was representative across our PMMA-transferred graphene electrodes and with this mediator.
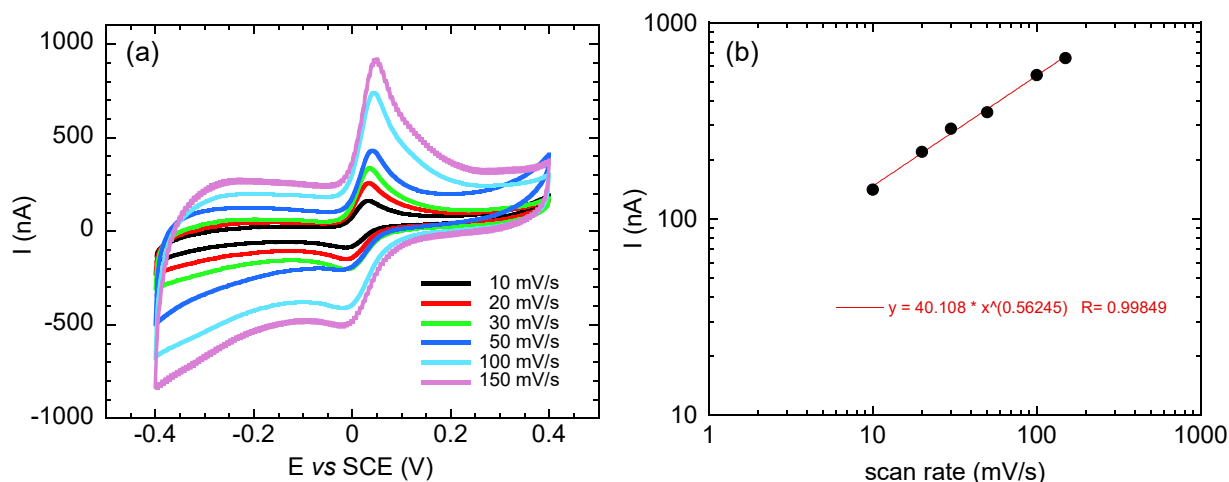

Figure S20: *(a) Cyclic voltammograms for CVD graphene in presence of 30 μM DCPIP in 10 ml reaction volume, as a function of scan rate. (b) The anodic current peak varies with the scan rate according to a power law with an exponent of ~ 0.56. Data in (b) were obtained from the peaks of the corresponding CV curves after baseline extraction.*

11. Microcontact printing/stamping protocol on graphene surfaces. *PDMS preparation:* Polydimethylsiloxane stamps were prepared by adding a curing agent (Dow Corning Sylgard 84) to a silicon master, in a 7:1 ratio. The mixture was poured into a mould in contact with a pattern created by photolithography with an 18/13 resist. Air was removed by putting the mould into a vacuum for 30 minutes, followed by overnight curing at 90°C in an oven.

Microcontact printing of E2 complexes was conducted using a patterned PDMS stamp which was incubated for 5 minutes with E2 complexes at room temperature from 0.1 mg/ml concentration stock solution, then dried on a filter paper with the active face upwards. This was followed by contact printing of graphene for 1 min, and subsequent sample drying with nitrogen.

(1) Heath, C.; Posner, M. G.; Aass, H. C.; Upadhyay, A.; Scott, D. J.; Hough, D. W.; Danson, M. J. The 2-Oxoacid Dehydrogenase Multi-Enzyme Complex of the Archaeon Thermoplasma Acidophilum − Recombinant Expression, Assembly and Characterization. *FEBS J.* **2007,** *274* (20), 5406-5415.

(2) Porollo, A. A.; Adamczak, R.; Meller, J. Polyview: A Flexible Visualization Tool for Structural and Functional Annotations of Proteins. *Bioinformatics* **2004,** *20* (15), 2460-2462.

(3) Bae, S.; Kim, H.; Lee, Y.; Xu, X.; Park, J.-S.; Zheng, Y.; Balakrishnan, J.; Lei, T.; Ri Kim, H.; Song, Y. I.; Kim, Y.-J.; Kim, K. S.; Ozyilmaz, B.; Ahn, J.-H.; Hong, B. H.; Iijima, S. Roll-to-Roll Production of 30-Inch Graphene Films for Transparent Electrodes. *Nat. Nanotechnol.* **2010,** *5* (8), 574-578.

(4) Dresselhaus, M. S.; Jorio, A.; Hofmann, M.; Dresselhaus, G.; Saito, R. Perspectives on Carbon Nanotubes and Graphene Raman Spectroscopy. *Nano Lett.* **2010,** *10* (3), 751-758.

(5) Yin, P.; Zhao, M.; Deng, C. High Efficiency Enrichment of Low-Abundance Peptides by Novel Dual-Platform Graphene@SiO$_2$@PMMA. *Nanoscale* **2012,** *4* (22), 6948-6950.

(6) Pham, V. H.; Cuong, T. V.; Hur, S. H.; Oh, E.; Kim, E. J.; Shin, E. W.; Chung, J. S. Chemical Functionalization of Graphene Sheets by Solvothermal Reduction of a Graphene Oxide Suspension in N-Methyl-2-Pyrrolidone. *J. Mater. Chem.* **2011,** *21* (10), 3371-3377.

(7) Horcas, I.; Fernández, R.; Gómez-Rodríguez, J. M.; Colchero, J.; Gómez-Herrero, J.; Baro, A. M. WSxM: A Software for Scanning Probe Microscopy and a Tool for Nanotechnology. *Rev. Sci. Instrum.* **2007,** *78* (1), 013705.

(8) Rabani, E.; Reichman, D. R.; Geissler, P. L.; Brus, L. E. Drying-Mediated Self-Assembly of Nanoparticles. *Nature* **2003,** *426* (6964), 271-274.

(9) Stannard, A.; Martin, C. P.; Pauliac-Vaujour, E.; Moriarty, P.; Thiele, U. Dual-Scale Pattern Formation in Nanoparticle Assemblies. *J. Phys. Chem. C* **2008,** *112* (39), 15195-15203.

(10) Ge, G.; Brus, L. Evidence for Spinodal Phase Separation in Two-Dimensional Nanocrystal Self-Assembly. *J. Phys. Chem. B* **2000,** *104* (41), 9573-9575.

(11) Tang, J.; Ge, G.; Brus, L. E. Gas−Liquid−Solid Phase Transition Model for Two-Dimensional Nanocrystal Self-Assembly on Graphite. *J. Phys. Chem. B* **2002,** *106* (22), 5653-5658.

(12) García, R.; Pérez, R. Dynamic Atomic Force Microscopy Methods. *Surf. Sci. Rep.* **2002,** *47* (6–8), 197-301.

(13) Viani, M. B.; Pietrasanta, L. I.; Thompson, J. B.; Chand, A.; Gebeshuber, I. C.; Kindt, J. H.; Richter, M.; Hansma, H. G.; Hansma, P. K. Probing Protein-Protein Interactions in Real Time. *Nat. Struct. Mol. Biol.* **2000,** *7* (8), 644-647.

(14) Müller, D. J.; Engel, A. The Height of Biomolecules Measured with the Atomic Force Microscope Depends on Electrostatic Interactions. *Biophys. J.* **1997,** *73* (3), 1633-1644.

(15) Garcia, R.; San Paulo, A. Attractive and Repulsive Tip-Sample Interaction Regimes in Tapping-Mode Atomic Force Microscopy. *Phys. Rev. B* **1999,** *60* (7), 4961-4967.

(16) Israelachvili, J., *Intermolecular & Surface Forces*. 2nd ed.; Academic Press: London, **1985**.

(17) Ishigami, M.; Chen, J. H.; Cullen, W. G.; Fuhrer, M. S.; Williams, E. D. Atomic Structure of Graphene on SiO$_2$. *Nano Lett.* **2007,** *7* (6), 1643-1648.

(18) Pirkle, A.; Chan, J.; Venugopal, A.; Hinojos, D.; Magnuson, C. W.; McDonnell, S.; Colombo, L.; Vogel, E. M.; Ruoff, R. S.; Wallace, R. M. The Effect of Chemical Residues on the Physical and Electrical Properties of Chemical Vapor Deposited Graphene Transferred to SiO$_2$. *Appl. Phys. Lett.* **2011,** *99* (12), 122108.

(19) Levesque, P. L.; Sabri, S. S.; Aguirre, C. M.; Guillemette, J.; Siaj, M.; Desjardins, P.; Szkopek, T.; Martel, R. Probing Charge Transfer at Surfaces Using Graphene Transistors. *Nano Lett.* **2011,** *11* (1), 132-137.

(20) Chen, J.-H.; Jang, C.; Xiao, S.; Ishigami, M.; Fuhrer, M. S. Intrinsic and Extrinsic Performance Limits of Graphene Devices on SiO$_2$. *Nat. Nanotechnol.* **2008,** *3* (4), 206-209.

(21) Yu Wang, Y.; Burke, P. J. A Large-Area and Contamination-Free Graphene Transistor for Liquid-Gated Sensing Applications. *Appl. Phys. Lett.* **2013,** *103* (5), 052103.

(22) Chen, T.-Y.; Loan, P. T. K.; Hsu, C.-L.; Lee, Y.-H.; Tse-Wei Wang, J.; Wei, K.-H.; Lin, C.-T.; Li, L.-J. Label-Free Detection of DNA Hybridization Using Transistors Based on CVD Grown Graphene. *Biosens. Bioelectron.* **2013,** *41* (0), 103-109.

(23) Stephens, P. E.; Darlison, M. G.; Lewis, H. M.; Guest, J. R. The Pyruvate Dehydrogenase Complex of Escherichia Coli K12. *Eur. J. Biochem.* **1983,** *133* (3), 481-489.

(24) Ma, F.; Zhang, Z.; Jia, H.; Liu, X.; Hao, Y.; Xu, B. Adsorption of Cysteine Molecule on Intrinsic and Pt-Doped Graphene: A First-Principle Study. *J. Mol. Struct.: THEOCHEM* **2010,** *955* (1–3), 134-139.

(25) Chen, R. J.; Bangsaruntip, S.; Drouvalakis, K. A.; Wong Shi Kam, N.; Shim, M.; Li, Y.; Kim, W.; Utz, P. J.; Dai, H. Noncovalent Functionalization of Carbon Nanotubes for Highly Specific Electronic Biosensors. *P. Natl. Acad. Sci. U.S.A.* **2003,** *100* (9), 4984-4989.

(26) Allen J. Bard , L. R. F., Electrochemical Methods : Fundamentals and Applications. New York ; Chichester : John Wiley New York.

(27) Heinze, J. Cyclic Voltammetry—"Electrochemical Spectroscopy". New Analytical Methods (25). *Angew. Chem., Int. Ed.* **1984,** *23* (11), 831-847.

(28) Fradet, E.; Abbyad, P.; Vos, M. H.; Baroud, C. N. Parallel Measurements of Reaction Kinetics Using Ultralow-Volumes. *Lab on a Chip* **2013,** *13* (22), 4326-4330.